Energy Efficient Pneumatics: Aspects of Control and Systems Theory

Daniel Müller*, Jonathan Haag, Jennifer Wickert, Adrian Raisch, Kathrin Hoffmann, Kevin Schmidt and Oliver Sawodny

Institute for System Dynamics (ISYS), University of Stuttgart, Waldburgstr. 17/19, 70563 Stuttgart, Germany
E-mail: daniel.mueller@isys.uni-stuttgart.de
**Corresponding Author*

Received 11 August 2021; Accepted 13 June 2022;
Publication 08 September 2022

Abstract

As the public call for increasing efforts in achieving the global climate protection goals intensifies, discussions about the efficient use of resources and energy are on the daily agenda. As many other areas, the industry has seen itself facing growing concerns about the long neglected environmental aspects. Since a large proportion of the energy in production is used by pneumatic drives, this survey paper exclusively focuses on pneumatics in handling and automation technology and presents the most common components, followed by multiple model-based strategies to increase energy efficiency in modern production plants.

First, single units are studied extensively and methods for design and energy efficient control are presented. Since in production lines pneumatic drives are generally operated in large networks, the second part focuses on energy efficient strategies at plant level. These include an optimized adjustment of the supply pressure, a cascaded air usage, and an automated adaptive control pattern. Care is taken to ensure that the considered approaches are

International Journal of Fluid Power, Vol. 23_3, 299–342.
doi: 10.13052/ijfp1439-9776.2333

applicable in today's industrial plants, which is demonstrated by experiments in a production line. The experimental findings show the immense potential of the discussed measures in the form of compressed air savings of more than 60% compared to the industry standard.

Keywords: Pneumatics, energy efficiency, control engineering, pressurized-air networks.

1 Introduction

Global warming has become one of the most, if not the most, important human challenges of the twenty-first century. Increasing environmental awareness and as a result rising energy prices have led to a demand of energy efficient technologies over the past years. As illustrated in Figure 1(a), industry is responsible for about 736 TWh equaling about 30% of total energy consumption in Germany. This demonstrates its significant role in achieving the global climate protection goals.

Compressed air and pneumatic drives play an important role in automation technology. They offer a lot of advantages compared to electrical or hydraulic actuators in a broad range of use cases due to their high power-density and environmental friendliness. This is why approximately 7–10% of the power demand in industry is related to pneumatic applications such as suction and blast air or pick and place tasks [3]. When considering the energy consumption of drive systems only, the share of pneumatics increases to roughly one fifth, as presented in Figure 1(b). However, due to

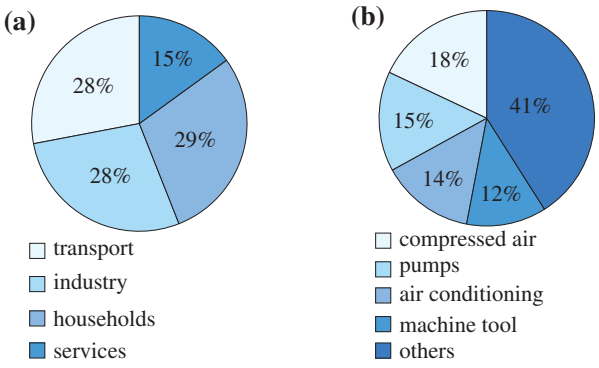

Figure 1 (a) Distribution of the total energy consumption by sectors in Germany [1], (b) electrical energy consumption of drive systems in Germany [2].

leakage-induced losses, inefficient control strategies and unfavorable dimensioning of pneumatic components, most processes relying on compressed air run inefficiently. This raises the question of how to enhance energy efficiency and consequently climate friendliness of pneumatic drive systems.

This paper presents a survey of optimization-based methods from a control and systems theory perspective to further improve energy efficiency of individual pneumatic drives as well as pressurized-air networks.

1.1 State of the Art

When examining the efficiency of pressurized air units, total cost of ownership (TCO) and life cycle assessments (LCA) have become common methods over the past few years. TCO enables the comparison of different drive technologies by converting consumed pressurized air to an equivalent amount of electrical energy [4] and taking other occurring costs into account, e.g., for maintenance and installation [5–7]. Using a similar approach, LCA considers the environmental impact of a product and has become increasingly important as efficiency requirements have risen [8]. Pneumatic drive systems are investigated using these techniques in [9], whereas [10] focuses on methods for power evaluation and [11] covers fluid actuators in general. In [12] not only production and operation but also decommissioning is examined concerning its ecological implications. Detailed comparisons of pneumatic and electromechanical drives are found in [13], [14] and [15].

Today, compressed air units are used in a variety of industrial applications, as the initial costs are typically much lower compared to electrical drives. Still, there remain two main areas offering significant room for improvement in terms of energy efficiency: accurate dimensioning and efficient control. An overview of different measures with respect to these topics is presented in [16] and [17].

In practice, pneumatic drives such as cylinders are usually chosen based on engineering experience or simple formulas provided by the manufacturers [18–20]. Furthermore, larger assemblies of pneumatic actuators generally operate more reliable, whereas the acquisition costs are only slightly higher. This is problematic though, as it leads to oversizing and as a consequence pneumatic drives are attributed efficiencies below 10% in many cases [21–23]. The use of exergy instead of energy stands to reason, as the former allows a reasonable assessment of potential losses [24–26].

Optimal sizing of individual cylinders based on a given motion task is discussed in [27] and [28]. While both articles show enormous energy saving

potential, they rely on numerically inefficient optimization schemes, making them impracticable for users. In contrast, the authors of [29, 30] promote the use of the cylinder eigenfrequency as an easily determinably variable allowing the selection of reasonable sized units. Another interesting approach is proposed in [31] by means of operating point analysis, however the focus of this article is less on optimal sizing but rather on parameter sensitivity with respect to maximum efficiency. Furthermore, the Association of German Engineers (VDI, for ger. *Verein Deutscher Ingenieure*) has published a standardized procedure to evaluate and select pneumatic drives [32].

With the goal of lowering the air consumption by optimizing the motion profile, methods of efficient control have been studied more extensively. Based on input/output-linearization to compensate for the system nonlinearities [33], different strategies to generate efficient trajectories are discussed in [34], [35], and [36]. An additional assessment of the profitability using TCO is presented in [37]. While all of the aforementioned control-related publications use proportional valves, [38], [39], and [40] apply position-based control with switch valves in pulse width modulation mode. In [41], a partial position information at the ends of the cylinder stroke is considered.

Switch-valve-based control for pneumatic cylinders in general has been investigated in multiple works [42–45]. Reference paper [46] utilizes optimal open-loop control to reduce energy consumption and is expanded upon an adaptation mechanism in [47].

When dealing with pneumatic networks, it is common to dispense with simulations of individual drives and instead use an abstract model of compressed air consumers [48]. By doing so, it is not only possible to create models of entire production plants [49, 50], but also to design and evaluate them accurately [51–53]. However, while these publications focus more on the supply of compressed air, this work is concerned with the energy saving potential of operating multiple pneumatic drives simultaneously [54]. This topic is mostly ignored in literature, only a few authors consider the reuse of exhaust air [55–57].

The results from [30] and [58] are of great significance for this work, since they analyze dimensioning and optimal control of individual drives and pneumatic networks, respectively.

1.2 Contribution and Structure of the Article

This paper presents an overview of modeling pneumatic production units ranging from individual components to entire networks. Moreover, practical

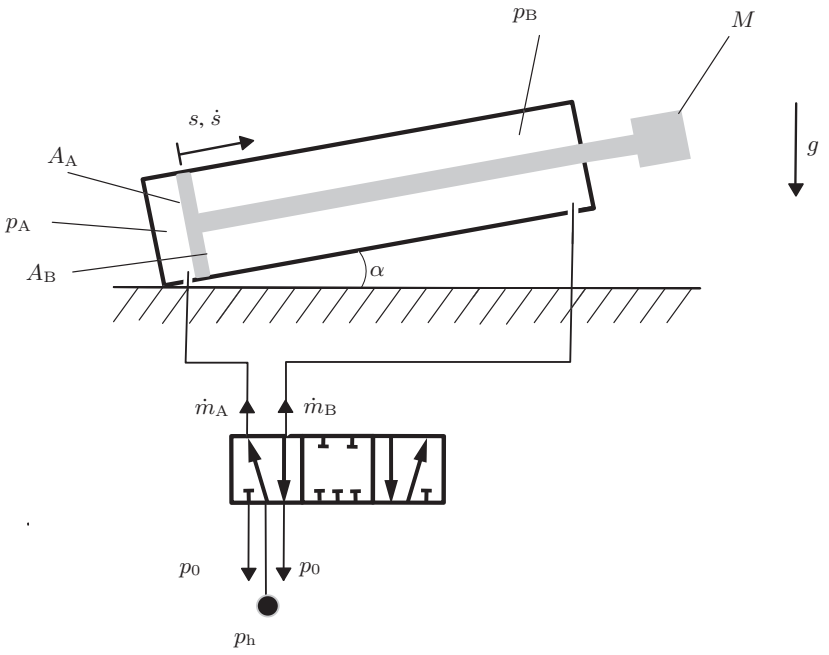

Figure 2 Schematic sketch of a pneumatic cylinder connected to a 5/3 valve.

energy saving measures are proposed in the form of optimization algorithms focusing on dimensioning and efficient control. The suggested methods show notable improvements and are worth consideration when designing factories containing compressed air systems. Not only are they applicable to single pneumatic drives but remain practicable when dealing with entire production plants. Essential results are also to be found in [54, 59]. All simulation results are obtained using MATLAB/Simulink, and experimental results are presented as well.

The remainder of the article is organized as follows: Section 2 introduces detailed models of pneumatic cylinders, valves, and pneumatic networks. Following, strategies on minimizing the energy consumption of individual drives (Section 3) and pressurized-air networks (Section 4) are described. Finally, the results are summarized in Section 5.

2 Modeling Components and Pressurized-air Networks

This section focuses on the derivation of detailed models of individual pneumatic components. Section 2.1 presents mechanical and thermodynamical

modeling approaches regarding pneumatic cylinders, while Sections 2.2 and 2.3 focus on the mass flow through valves and tubes. The resulting models for the cylinder and valves are later used for optimization, therefore their accuracy is crucial. Although the tubing model is not considered in the following chapters, it is included to present a complete general model of pneumatic systems.

2.1 Modeling of Pneumatic Cylinders

For a pneumatic cylinder of length l as shown in Figure 2, a mechanical model is derived using Newton's law. Given the pressures $p_{\mathrm{A}}(t)$ and $p_{\mathrm{B}}(t)$, the resulting equation of motion is

$$\begin{aligned} M\ddot{s}(t) =& A_{\mathrm{A}}p_{\mathrm{A}}(t) - A_{\mathrm{B}}p_{\mathrm{B}}(t) - (A_{\mathrm{A}} - A_{\mathrm{B}})p_0 - F_{\mathrm{H}}(t) - F_{\mathrm{G}} \\ & - F_{\mathrm{F}}\big(\dot{s}(t)\big) - F_{\mathrm{T}}\big(s(t), \dot{s}(t)\big), \end{aligned} \tag{1}$$

where $s(t)$ is the position of the piston and M describes the load mass. The holding force F_{H} describes the force that is applied to an external object, its minimum amount is usually determined by the motion task. The piston area and pressure of the two chambers are represented by A_i and p_i with $i \in \{\mathrm{A}, \mathrm{B}\}$, while p_0 is the ambient pressure. Moreover, the gravitational force F_{G}, the friction force F_{F}, and the terminal force F_{T} are modeled as

$$F_{\mathrm{G}} = Mg\sin(\alpha), \tag{2a}$$

$$F_{\mathrm{F}}(\dot{s}) = \tanh\left(\frac{\dot{s}}{\nu_{\mathrm{G}}}\right)\left(f_{\mathrm{C}} + (f_{\mathrm{S}} - f_{\mathrm{C}})\exp\left[-\left|\frac{\dot{s}}{\nu_{\mathrm{S}}}\right|^{\delta_{\mathrm{S}}}\right]\right) + f_{\mathrm{V}}\dot{s}, \tag{2b}$$

$$F_{\mathrm{T}}(s, \dot{s}) = \begin{cases} \gamma|s|^{\beta}\dot{s} - \delta|s|^{\beta}, & s \leq 0 \\ 0, & s \in (0, l) \\ \gamma|l - s|^{\beta}\dot{s} - \delta|l - s|^{\beta}, & s \geq l, \end{cases} \tag{2c}$$

with the mounting orientation α, friction parameters f_{C}, f_{S}, and f_{V}, a shape parameter δ_{S}, the transition velocity ν_{G} as well as Stribeck velocity ν_{S}. The presented friction model is based on [60], an advanced model can be found in [61]. The Hunt-Crossley contact force model used in (2c) is derived in [62] and contains design parameters β, γ, and δ.

Furthermore, a thermodynamical model of the cylinder is derived using the first law of thermodynamics for open systems [30]:

$$\dot{U}_i = \dot{Q}_i + \dot{H}_i + \dot{W}_i. \tag{3}$$

The change of the internal energy $\dot{U}_i$, the heat flow $\dot{Q}_i$, the enthalpy $\dot{H}_i$, and the work for volume change $\dot{W}_i$ are obtained using

$$i \in \{\mathrm{A}, \mathrm{B}\}: \qquad \dot{U}_i = \frac{c_v}{R_L}(p_i \dot{V}_i + V_i \dot{p}_i), \tag{4a}$$

$$\dot{Q}_i = \alpha_T A_i (\theta_i - \theta_0), \tag{4b}$$

$$\dot{H}_i = \dot{m}_{i,\mathrm{I}} h_{i,\mathrm{I}} - \dot{m}_{i,\mathrm{O}} h_{i,\mathrm{O}}, \tag{4c}$$

$$\dot{W}_i = -p_i \dot{V}_i. \tag{4d}$$

Here, V_i is the chamber volume with the corresponding absolute temperature θ_i, the mass flows $\dot{m}_{i,j}$ and enthalpies $h_{i,j} = c_p \theta_{i,j}$ of the in- ($j = \mathrm{I}$) and outflowing ($j = \mathrm{O}$) air. Note that the inflowing air has ambient temperature and the outflowing air the temperature of the respective chamber, i.e., $\theta_{i,\mathrm{I}} = \theta_0$ and $\theta_{i,\mathrm{O}} = \theta_i$. Additionally, R_L denotes the specific gas constant, α_T the heat transfer coefficient and c_v and c_p the heat capacities for constant volume and pressure.

To reduce the model complexity for optimization and controller design, polytropic state transitions are assumed in the following. Since the polytropic exponent n implicitly describes the heat transfer, the temperature dynamics is neglected and instead only the temperature of the inflowing air θ_0 is considered. As shown in [63], this assumption is valid. Together with (4a)–(4d) plugged into (3), the pressure dynamics results in

$$\dot{p}_i = \frac{n}{V_i(s)} \left(R_L \theta_0 \dot{m}_i - \dot{V}_i(\dot{s}) p_i \right), \quad i \in \{A, B\} \tag{5}$$

with $\dot{m}_i = \dot{m}_{i,\mathrm{I}} - \dot{m}_{i,\mathrm{O}}$ and $n \in [1, \kappa]$, where $\kappa = c_p/c_v$ describes the isentropic exponent.

2.2 Modeling the Mass Flow Through Valves

In this section, a brief description of the functionality and modeling of common industrial valves is given. They are distinguished between proportional valves and switching valves. While the latter ones solely realize a discrete set of valve positions, e.g., fully opened or closed, the sonic conductance of proportional valves is continuously adjustable [30, 64, 65]. As a result switching valves are generally the cheaper option and therefore widely used in industrial applications which is why only switching valves are considered in the following.

In Figure 2, a 5/3 switching valve is depicted at the bottom. The nomenclature is defined as follows: The first number, in this case '5', denotes the

number of in- and outports, whereas the second number, in this case '3', denotes the number of possible switching positions. A useful feature of 5/3 valves is their ability to provide and simultaneously dissipate pressure flows. As shown in Figure 2, in the leftmost position the supply pressure is directed towards chamber A while chamber B is vented. The user can switch between positions by shifting an internal spool. If the valve is connected to a cylinder, as it is the case in Figure 2, its piston extends using the left position and retracts using the right position.

Valves are modeled as throttles and a general description of the mass flow through a valve is given by [66]

$$\dot{m} = \rho p_{\mathrm{prim}} C \psi \left(\frac{p_{\mathrm{sec}}}{p_{\mathrm{prim}}}, b \right), \tag{6}$$

with density ρ of the fluid, sonic conductance C of the valve, flow function ψ and critical pressure ratio b. The index 'prim' denotes the inflowing pressure, while 'sec' denotes the outflowing pressure. The sonic conductance is computed as the inverse of the flow resistance and thus describes how efficiently the fluid is being transported through the valve despite friction. Hence, different links through the valve lead to different conductivities. As long as the pressure ratio is below the critical ratio b the air flows with speed of sound otherwise it slows down which is considered by the flow function

$$\psi \left(\frac{p_{\mathrm{sec}}}{p_{\mathrm{prim}}}, b \right) = \begin{cases} \sqrt{1 - \left(\frac{\frac{p_{\mathrm{sec}}}{p_{\mathrm{prim}}} - b}{1 - b} \right)^2} & \frac{p_{\mathrm{sec}}}{p_{\mathrm{prim}}} \geq b \\ 1 & \text{else} \end{cases}. \tag{7}$$

Under the assumption of a frictionless air flow and an adiabatic process the critical pressure ratio b is computed to

$$b = \left(\frac{2}{\kappa + 1} \right)^{\frac{\kappa}{\kappa + 1}} = 0.528. \tag{8}$$

In order to obtain accurate control results, the experimental identification of the critical pressure ratio stands to reason, as the relation (7) is an approximation itself [64].

2.3 Modeling Pneumatic Tubes

Modeling the mass flow in (6) is based on the assumption of a spatially constant mass flow $\dot{m}$, which does not change from entering to leaving the

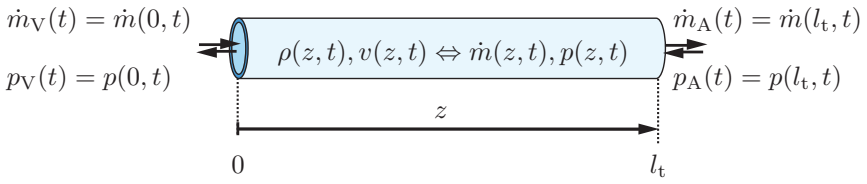

Figure 3 The flow within a tube of length l_{t}, which connects a valve (index V) to a pressure chamber (index A), can be modeled either by the spatially distributed states density $\rho(z,t)$ and flow speed $v(z,t)$ or by the mass flow $\dot{m}(z,t)$ and the pressure $p(z,t)$, see [64].

valve. Certainly, this argumentation is reasonable for short tubes that connect components in a pneumatic network. However, the transport time as well as dynamic behavior increase with longer tubes. In the following, an ordinary differential equation (ODE) is derived from a spatially distributed model describing the dynamics of air flow through tubes [64, 67].

Starting with the conservation laws of mass and momentum for compressible fluids, one obtains a set of nonlinear partial differential equations (PDEs) for the flow speed $v(z,t)$ and the density $\rho(z,t)$ within the tube $z \in (0, l_{\mathrm{t}})$

$$\text{mass:} \qquad \frac{\partial \rho}{\partial t} + \frac{\partial (\rho v)}{\partial z} = 0 \tag{9a}$$

$$\text{momentum:} \qquad \frac{\partial (\rho v)}{\partial t} + \frac{\partial}{\partial z}\left(\rho v^2 + p\right) = -p_{\mathrm{F}}, \tag{9b}$$

where p_{F} is a friction term [68]. The above PDEs are the one-dimensional formulation of the well-known Navier-Stokes equations.

For the application in the field of pneumatics, it is more convenient to simplify and reformulate (9) in terms of mass flow $\dot{m} = A_{\mathrm{t}} \rho v$ and the pressure $p = c^2 \rho$ respectively. Note that the constant cross section of the tube and the speed of sound are denoted by A_{t} and c. Given further mild assumptions, such as an inelastic tube; no thermodynamical interaction between gas and wall; the following set of linear PDEs approximates (9) for small deviations w. r. t. the stationary solution [52, 64]. Together with the boundary and initial conditions (BC, IC) shown in Figure 3, the distributed parameter system is well-posed:

$$\text{PDEs}: \qquad \frac{1}{A_{\mathrm{t}}} \frac{\partial \dot{m}(z,t)}{\partial t} = -R_{\mathrm{t}} \dot{m}(z,t) - \frac{\partial p(z,t)}{\partial z} \tag{10a}$$

$$\frac{A_{\mathrm{t}}}{c^2} \frac{\partial p(z,t)}{\partial t} = -\frac{\partial \dot{m}(z,t)}{\partial z}, \qquad z \in (0, l_{\mathrm{t}}), t > 0 \tag{10b}$$

$$\text{BCs:} \qquad \dot{m}(0,t) = \dot{m}_{\mathrm{V}}(t) \tag{10c}$$

$$p(l_{\mathrm{t}},t) = p_{\mathrm{A}}(t), \quad \text{for } t \geq 0 \tag{10d}$$

$$\text{ICs:} \qquad \dot{m}(z,0) = 0, \tag{10e}$$

$$p(z,0) = p_0(z), \quad \text{for } z \in [0,l_t] \tag{10f}$$

Boundary conditions are chosen such that they describe the mass inflow coming from the valve and the target pressure at the chamber, while the initial conditions describe a stationary point. The outputs of the tube are $y_1(t) = \dot{m}(l_{\mathrm{t}},t) = \dot{m}_{\mathrm{A}}(t)$ and $y_2(t) = p(0,t) = p_{\mathrm{V}}(t)$.

An approximation of the analytical solution is now derived, which describes the first mode exactly [64], yielding the following linear state space representation

$$\frac{\mathrm{d}}{\mathrm{d}t}\begin{bmatrix}\dot{m}_{\mathrm{A}}\\ p_{\mathrm{V}}\end{bmatrix} = \begin{bmatrix}-l_{\mathrm{t}}R_{\mathrm{t}} & \frac{A_{\mathrm{t}}}{l_{\mathrm{t}}}\\ -\frac{c^2\pi^2}{4A_{\mathrm{t}}l_{\mathrm{t}}} & 0\end{bmatrix}\begin{bmatrix}\dot{m}_{\mathrm{A}}\\ p_{\mathrm{V}}\end{bmatrix} + \begin{bmatrix}0 & -\frac{A_{\mathrm{t}}}{l_{\mathrm{t}}}\\ \frac{c^2\pi^2}{4A_{\mathrm{t}}l_{\mathrm{t}}} & 0\end{bmatrix}\begin{bmatrix}\dot{m}_{\mathrm{V}}\\ p_{\mathrm{A}}\end{bmatrix}. \tag{11}$$

Due to high velocities in the tube, the flow is turbulent and therefore a nonlinear friction term is added to Equation (11). The upper left entry $-l_{\mathrm{t}}R_{\mathrm{t}}$ of the system matrix in Equation (11) is a damping term, which is replaced by the throttling model from Equation (6). Rearranging (6) and inverting the outflow function (7) yields

$$\Delta p = \psi^{-1}(p_{\mathrm{A}}, \dot{m}_{\mathrm{A}}, C_{\mathrm{t}}, b_{\mathrm{t}}, \rho) - p_{\mathrm{A}}. \tag{12}$$

The nonlinear model describing turbulent flows is then [67]

$$\frac{\mathrm{d}}{\mathrm{d}t}\begin{bmatrix}\dot{m}_{\mathrm{A}}\\ p_{\mathrm{V}}\end{bmatrix} = \begin{bmatrix}0 & \frac{A_{\mathrm{t}}}{l_{\mathrm{t}}}\\ -\frac{c^2\pi^2}{4A_{\mathrm{t}}l_{\mathrm{t}}} & 0\end{bmatrix}\begin{bmatrix}\dot{m}_{\mathrm{A}}\\ p_{\mathrm{V}}\end{bmatrix} + \begin{bmatrix}0 & -\frac{A_{\mathrm{t}}}{l_{\mathrm{t}}}\\ \frac{c^2\pi^2}{4A_{\mathrm{t}}l_{\mathrm{t}}} & 0\end{bmatrix}\begin{bmatrix}\dot{m}_{\mathrm{V}}\\ p_{\mathrm{A}}\end{bmatrix} + \begin{bmatrix}-\frac{A_{\mathrm{t}}}{l_{\mathrm{t}}}\\ 0\end{bmatrix}\Delta p. \tag{13}$$

This description is applicable to tubes with $10\,\mathrm{cm} \leq l_{\mathrm{t}} \leq 6\,\mathrm{m}$ and chambers of at least ten times the volume of the tube [64].

3 Minimizing the Energy Consumption of Individual Drives

Since cylinders with larger dimensions are only slightly more expensive, but improve robustness against leakage, most compressed air units tend to be oversized. For example, doubling the piston diameter increases the purchase

price by just 18% in some cases [69]. Note that the task specific parameters like the load mass, transition time and boundary conditions are typically specified by system designers in practice. As a consequence, these parameters are assumed to be known and used in the following for dimensioning the pneumatic units.

In a similar fashion, the standard control patterns for the cylinder chambers are either fully aerating or venting. While this is a simple strategy which again improves robustness against leakage, it is also energy inefficient.

Thus, the key goal is to find design parameters such that a given motion task is performed while energy consumption is minimized. Two measures providing the most energy saving potential for pressurized air applications have been identified: Firstly reducing the required amount of used air by choosing properly sized cylinders and secondly maximizing the proportion of expansion work by optimizing control patterns.

3.1 Model-based Optimal Sizing of Pneumatic Cylinders

For each individual drive and a corresponding motion task a well suited drive configuration, i.e., cylinder size, supply pressure, and valves, has to be selected such that the overall process is as energy efficient as possible. The proposed methods to do so, that are presented in this section, are largely based on the results of [59] and [70]. Note that these references also offer more detailed explanations and implementation details. In this article, the measure for energy efficiency is given by the air consumption of compressed air for isothermal processes with a polytropic exponent of $n = 1$

$$\begin{aligned} J &= \frac{1}{\rho_0} \int_0^T \dot{m}_{\mathrm{A}}^+(\tau) + \dot{m}_{\mathrm{B}}^+(\tau) \mathrm{d}\tau, \\ &= \frac{1}{p_0} \left((V_{0,\mathrm{A}} + V_{0,\mathrm{B}})(p_{\mathrm{h}} - p_0) + (A_{\mathrm{A}} + A_{\mathrm{B}}) l p_{\mathrm{h}} \right), \end{aligned} \tag{14}$$

with the positive shares of the mass flow

$$\dot{m}_i^+(t) = \begin{cases} \dot{m}_i(t) & \text{if } \dot{m}_i(t) > 0 \\ 0 & \text{else,} \end{cases} \tag{15}$$

cycle time T with $s(T) = l$, air density ρ_0, ambient pressure p_0 and initial volume $V_{0,i}$. Its unit is given by $[J] = \mathrm{N}\ell$ (standard liters). Note that for the optimal sizing problem the standard control pattern is assumed, i.e., the

chambers of the cylinders are either aerated or vented. By considering n_A actuators supplied together, the dimensioning problem is formulated as an optimization problem

$$\min_{\boldsymbol{\zeta}_k} \sum_{k=1}^{n_\mathrm{A}} J_k \tag{16a}$$

$$\text{s.t.} \quad \dot{\boldsymbol{x}}_k = \boldsymbol{f}(\boldsymbol{x}_k, \boldsymbol{\zeta}_k, \boldsymbol{\Phi}_k), \quad \boldsymbol{x}_k(0) = \boldsymbol{x}_{0,k}(\boldsymbol{\zeta}_k), \tag{16b}$$

$$\boldsymbol{\zeta}_k[1] = p_\mathrm{h}, \qquad k = 1, \ldots, n_\mathrm{A}, \tag{16c}$$

$$\boldsymbol{g}(\boldsymbol{\zeta}_k) \leq 0, \tag{16d}$$

$$\boldsymbol{h}_k(\boldsymbol{x}_k, \boldsymbol{\zeta}_k) = \begin{bmatrix} F^*_{\mathrm{H},j_\mathrm{P},k} - F_{\mathrm{H},j_\mathrm{P},k}(\boldsymbol{\zeta}_k) \\ T_{j_\mathrm{P},k}(\boldsymbol{x}_k) - T^*_{j_\mathrm{P},k} \\ v_{j_\mathrm{P},k}(\boldsymbol{x}_k) - v^*_{j_\mathrm{P},k} \end{bmatrix} \leq 0, \tag{16e}$$

where (16b) describes the cylinder dynamics with state vector $\boldsymbol{x}(t) = [s(t), \dot{s}(t), p_\mathrm{A}(t), p_\mathrm{B}(t)]^\top \in \mathbb{R}^{n_\mathrm{x}}$, design variables $\boldsymbol{\zeta} = [p_\mathrm{h}, d, C^\mathrm{E}_\mathrm{A}, C^\mathrm{R}_\mathrm{A}, C^\mathrm{E}_\mathrm{B}, C^\mathrm{R}_\mathrm{B}]^\top \in \mathbb{R}^{n_\zeta}$ and task parameters $\boldsymbol{\Phi} = [m, \alpha]^\top \in \mathbb{R}^2$. The design variables are the supply pressure p_h, cylinder diameter d and valve conductances $C_i^{j_\mathrm{P}}$ with index j_P denoting a process of extension ($j_\mathrm{P} = \mathrm{E}$) or retraction ($j_\mathrm{P} = \mathrm{R}$). Constraint (16c) demands a common supply pressure for all cylinders while (16e) contains requirements for the holding force $F_{\mathrm{H},j_\mathrm{P},k}(\boldsymbol{\zeta}_k)$, which has to be greater or equal to a given force $F^*_{\mathrm{H},j_\mathrm{P},k}$, transition time $T_{j_\mathrm{P},k}(\boldsymbol{x}_k)$, which has to be smaller than operation time $T^*_{j_\mathrm{P},k}$ and impact velocity $v_{j_\mathrm{P},k}(\boldsymbol{x}_k) = \dot{s}(T_{j_\mathrm{P},k})$, which has to be smaller than the maximum allowed velocity $v^*_{j_\mathrm{P},k}$. Furthermore, (16d) allows consideration of additional conditions, for example a minimum supply pressure. Note that the cylinder diameter d is discrete valued as manufacturers typically offer a number of predetermined sizes.

To solve the optimization problem (16) a gradient approach is chosen. However, commonly used gradient-based algorithms do not deal with discrete-value sets of parameters, so the results have to be rounded to be applicable. Furthermore, to assess a parameter configuration $\bar{\boldsymbol{\zeta}}$ the cost functional J has to be evaluated which requires a simulation of the system (16b). This is computationally demanding, especially if the gradient is computed using finite differences. To overcome those issues, a gradient-based optimization scheme is proposed that works directly with discrete sets of parameters and provides its gradient at each iteration step.

The gradients of the cost function and the inequality constraints with respect to the design variables

$$\frac{\partial J}{\partial \boldsymbol{\zeta}} = \frac{\partial J}{\partial \boldsymbol{x}} \frac{\partial \boldsymbol{x}}{\partial \boldsymbol{\zeta}}, \qquad \frac{\partial \boldsymbol{h}}{\partial \boldsymbol{\zeta}} = \frac{\partial \boldsymbol{h}}{\partial \boldsymbol{x}} \frac{\partial \boldsymbol{x}}{\partial \boldsymbol{\zeta}} \tag{17}$$

both depend on the sensitivity $\boldsymbol{S}(t) = \frac{\partial \boldsymbol{x}}{\partial \boldsymbol{\zeta}}(t, \bar{\boldsymbol{\zeta}}, \boldsymbol{\Phi}) \in \mathbb{R}^{n_\mathrm{x} \times n_\zeta}$. While the gradient w. r. t. the system state $\boldsymbol{x}$ is calculated analytically, the sensitivity itself needs to be simulated at each iteration step ν of the optimization together with (16b) using the ODE:

$$\underbrace{\frac{\partial}{\partial \boldsymbol{\zeta}} \left(\frac{\mathrm{d}\boldsymbol{x}(t, \bar{\boldsymbol{\zeta}}, \boldsymbol{\Phi})}{\mathrm{d}t} \right)}_{=\dot{\boldsymbol{S}}(t)} = \frac{\partial \boldsymbol{f}(\boldsymbol{x}, \bar{\boldsymbol{\zeta}}, \boldsymbol{\Phi})}{\partial \boldsymbol{x}} \underbrace{\frac{\partial \boldsymbol{x}(t, \bar{\boldsymbol{\zeta}}, \boldsymbol{\Phi})}{\partial \boldsymbol{\zeta}}}_{=\boldsymbol{S}(t)} + \frac{\partial \boldsymbol{f}(\boldsymbol{x}, \bar{\boldsymbol{\zeta}}, \boldsymbol{\Phi})}{\partial \boldsymbol{\zeta}}, \tag{18}$$

and the initial condition $\boldsymbol{S}(0) = \partial \boldsymbol{x}(0) / \partial \boldsymbol{\zeta}$. Discretizing the remaining continuous design variables, namely the supply pressure and the valve conductances, yields a discrete-value set $\mathcal{P}$ of the design parameters $\boldsymbol{\zeta}$. By using the Taylor series

$$\boldsymbol{h}(\boldsymbol{x}(\bar{\boldsymbol{\zeta}} + \Delta\boldsymbol{\zeta}), \bar{\boldsymbol{\zeta}} + \Delta\boldsymbol{\zeta}) \approx \boldsymbol{h}(\boldsymbol{x}(\bar{\boldsymbol{\zeta}}), \bar{\boldsymbol{\zeta}}) + \underbrace{\left(\left. \frac{\partial \boldsymbol{h}}{\partial \boldsymbol{x}} \right|_{\bar{\boldsymbol{\zeta}}} \boldsymbol{S} + \left. \frac{\partial \boldsymbol{h}}{\partial \boldsymbol{\zeta}} \right|_{\bar{\boldsymbol{\zeta}}} \right)}_{=\boldsymbol{\Lambda}_\mathrm{h}^T} \Delta\boldsymbol{\zeta}, \tag{19}$$

the outcomes of the parameter variations $\Delta\boldsymbol{\zeta}$ in the neighbourhood of $\bar{\boldsymbol{\zeta}}$ are estimated by using the computationally cheap matrix-vector multiplication $\boldsymbol{\Lambda}_{\mathrm{h},\nu}^T \boldsymbol{P}_\nu$ where each column of $\boldsymbol{P}_\nu$ corresponds to a parameter configuration of the set $\mathcal{P}$. The same is done with regard to the cost function (14). The best predicted feasible configuration with respect to the cost is then chosen for the next iteration until convergence is archived. The proposed solution gives an accurate and fast result which allows the algorithm to run for instance as a web application providing support for system designers.

The baseline setting, to be compared to the results of the above optimization, is chosen according to industrial standards in [18], [19], [20], consisting of three cylinders. Experimental results using the baseline and the optimally dimensioned cylinders are summarized in Table 1 and show that the supply pressure as well as two of the three cylinder diameters are reduced. For values of the valve conductances, refer to [70], Table A.1. Further, measurement results showing the effects of the optimization in terms of position (normalized), pressure and air consumption are shown in Figure 4.

Table 1 Measurements of baseline and optimal dimensioning obtained from discrete scheme

Measurement	p_h in Bar	d_1 in mm	d_2 in mm	d_3 in mm	J in Nℓ
Baseline	4.8	32	20	12	4.40
Optimal	3.3	25	16	12	1.96

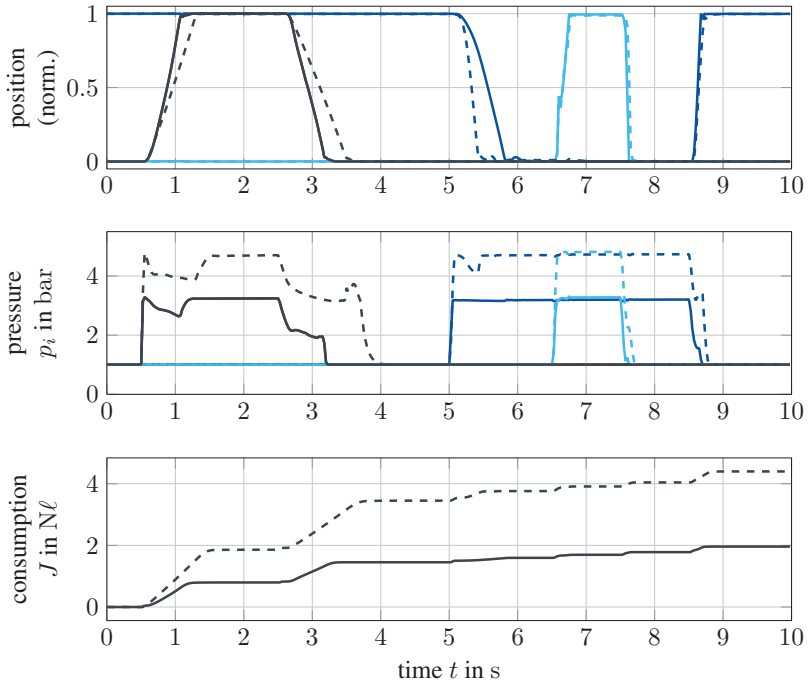

Figure 4 Measurement results of cylinders with optimization-based sizing. Positions (normalized), pressure and air consumption for drive 1 (—), drive 2 (—), and drive 3 (—) before (- -) and after (—) optimization are shown [70]. Note that the unit Nℓ refers to a standard reference atmosphere and is denoted in standard liters, see (14).

3.2 Online Adaptation of Control Patterns

Besides proper sizing, optimized operation is a method capable of reducing the energy intake of pneumatic cylinders. In this section, different control strategies and an online adaptation scheme are presented based on the results of [71].

3.2.1 Control strategies

The standard control strategy, already described above, is to aerate one chamber while simultaneously venting the other until the end position is

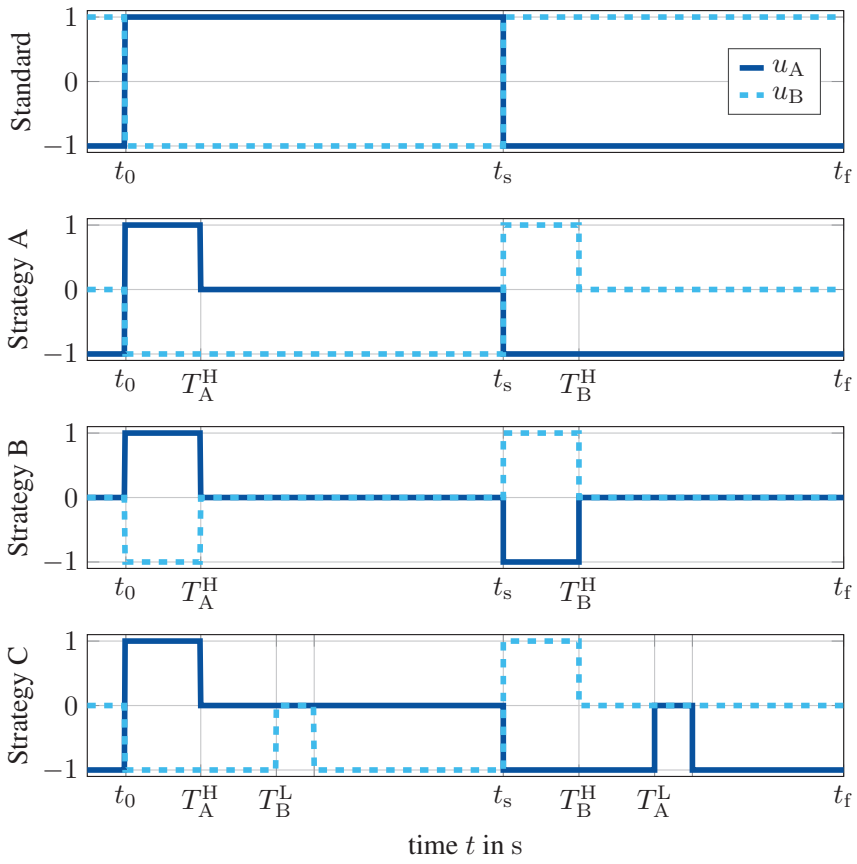

Figure 5 Standard control pattern and proposed strategies A, B and C [59].

reached. Because this approach is suboptimal in terms of air consumption and material stress (due to high impact velocities), different control policies are investigated regarding their energy saving potential. Thereby, it has to be ensured that transition time and robustness against variation of task parameters do not deteriorate. The main idea is to lower the air usage by maximizing the share of expansion work when performing a motion task.

A qualitative representation of the four considered strategies, Standard, A, B, and C, is shown in Figure 5, where $u_i \in \{-1, 0, 1\}$ determines if the chamber i is vented, closed or aerated. For one stroke, in this case extension, the differences of the proposed schemes are explained in the following: Strategy A stops aeration of chamber A at time T_A^H but continues to vent chamber

B. By doing so, the pressure level of chamber A does not increase as much as with the Standard strategy, but instead this approach prioritizes the use of the expansion potential of the pressurized air. As a result of giving it more time to expand, the amount of consumed air is significantly smaller compared to the Standard strategy while the motion task is still completed. However, the low pressure in chamber B still results in high impact velocities, especially for large cylinders. Strategy B stops both, aeration and venting, at the same time T_A^{H}. This strategy is in particular interesting since it only requires one 5/3 valve with blocking position. Strategy C combines the advantages of the first two, stopping aeration at time T_A^{H} and ventilation at T_B^{L}. As chamber B is vented longer than in Strategy B it does not require as much pressure in chamber A to assure complete extension. Simultaneously, impact speed is decreased compared to Strategy A, because venting of chamber B is blocked after T_B^{L} until the end position is reached, thus providing more effective damping. This manifests the broader applicability of Strategy C, though it needs the highest parametrization effort and relies on the most expensive hardware compared to the other strategies. Note that in the remainder of this section double strokes are examined – meaning one full extension followed by a complete retraction.

Optimal switching points for each policy are determined with the use of a genetic algorithm, leading to a significant decrease in compressed air consumption and in part even lower transition times as presented in Table 2. However, this time-based policy is not robust with respect to varying parameters, e.g., reduced or increased friction as a result of material wear. This may lead to high impact velocities or incomplete motions, which is why more robust control strategies are required. One important aspect of all considered approaches is their feasibility in realistic scenarios, especially in terms of additional hardware requirements and related costs. A rather simple adjustment to increase robustness is to carry out the above switching time-based optimization procedure, determine the piston position at the optimized switching times and then use these positions instead of time to determine when to switch. To implement this, only relatively cheap limit switches mounted at the corresponding intermediate positions are required to keep track of the piston movement. While this position-based approach can offset parameter variations in some scenarios, there are no guarantees for improvement, especially in the case of increased friction and incomplete motion tasks as a result thereof. This is why in the following an adaptive control scheme is considered which proves to be far more reliable in practice.

Table 2 Comparison of the energy consumption and transition times for extension and retraction for the different control patterns

Strategy	J in Nℓ	T_E in s	T_R in s
Standard	0.82	0.30	0.40
A	0.22	0.33	0.34
B	0.23	0.33	0.34
C	0.21	0.21	0.28

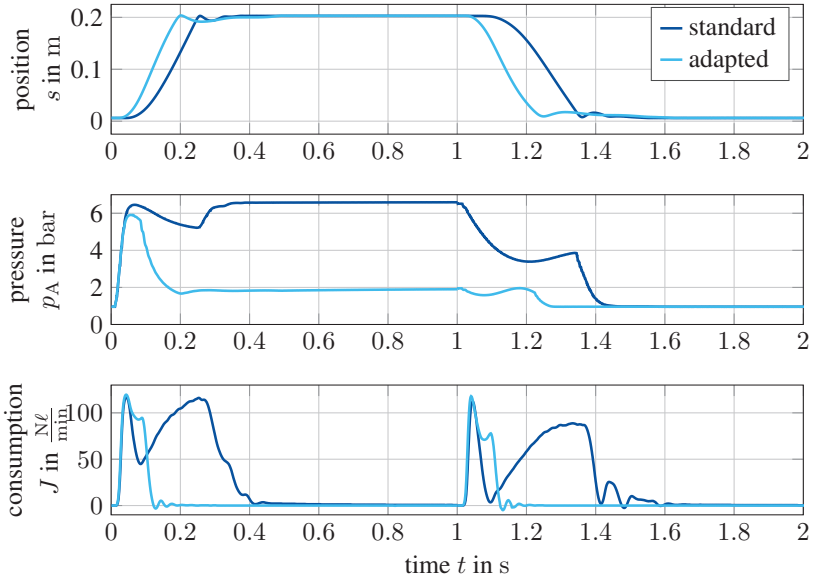

Figure 6 Measurement results of the online adaptation – state over time with continuous air supply (—) and after 17 adaptation cycles (—), see [54].

3.2.2 Adaptation law

As outlined in the previous paragraph, there is a need for robust, yet inexpensive control patterns. A typical approach to decrease sensitivity with respect to parameters is to use adaptive strategies that rely on model-based predictions of the system behavior. However, these strategies require additional sensors. To avoid the cost of any additional sensors and to increase robustness, a model-free online adaptation is introduced and tested in simulations and experiments.

In this paragraph, Strategy A is used as an example and the constraint regarding the impact velocity is neglected – an assumption that is fulfilled in most practical applications.

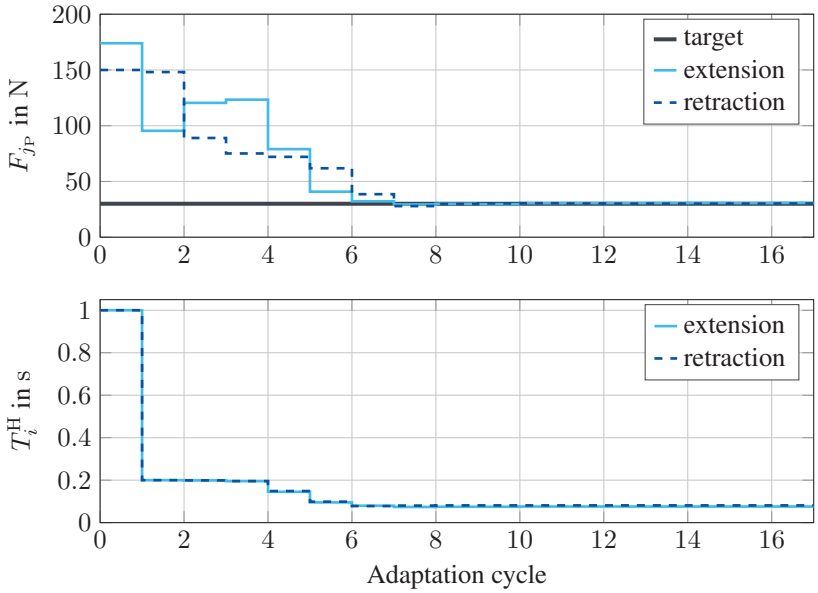

Figure 7 Measurement results of the holding forces and switching times for the adaptive scheme.

To obtain the ideal switching points T_i^{H}, when aeration is stopped, two independent optimization problems

$$\min_{T_i^{\mathrm{H}}} T_i^{\mathrm{H}} \tag{20a}$$

$$\text{s.t.} \quad \tilde{\boldsymbol{h}}_i(T_i^{\mathrm{H}}) = \begin{bmatrix} F_{j_{\mathrm{P}}}^* - F_{j_{\mathrm{P}}}(T_i^{\mathrm{H}}) \\ T_{j_{\mathrm{P}}}(T_i^{\mathrm{H}}) - T_{j_{\mathrm{P}}}^* \end{bmatrix} \leq 0. \tag{20b}$$

for extension ($j_{\mathrm{P}} = \mathrm{E}$, $i = \mathrm{A}$) and retraction ($j_{\mathrm{P}} = \mathrm{R}$, $i = \mathrm{B}$) have to be solved. Larger switching times lead to an increase in holding force and a decrease in transition time, so for constraint (20b) the inequality

$$\frac{\partial\, \tilde{\boldsymbol{h}}_i}{\partial T_i^{\mathrm{H}}} \leq 0, \tag{21}$$

holds. Since the overall goal is to minimize compressed air consumption, the switching time $T_i^{\mathrm{H}*}$ is determined such that all constraints (20b) are satisfied, i.e., $\max(\tilde{\boldsymbol{h}}_i(T_i^{\mathrm{H}*})) = 0$. This is the earliest time at which both constraints are met and thus the optimal solution for (20). For online computation a line-search algorithm is used.

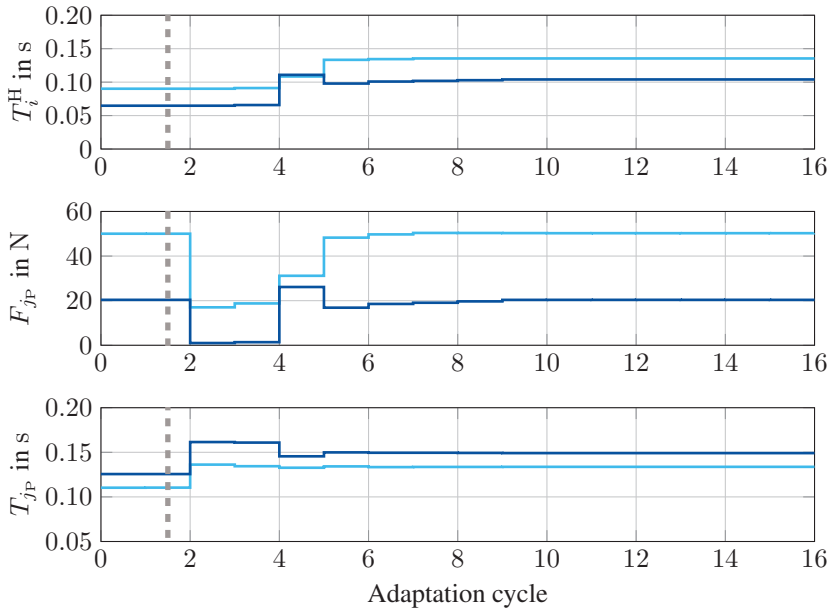

Figure 8 Simulation results of the adaptation law for drop in supply pressure (– –). Switching times, holdings forces and transition times for extension (—) and retraction (—) are shown.

The adaptation mechanism is tested and compared experimentally against the Standard strategy. Figure 6 shows the measurement results of the piston position, pressure and inflowing air for one transition of the Standard strategy and Strategy A after 17 adaptation cycles. The corresponding holding forces and switching times are shown in Figure 7.

To further test the extended control pattern, its adaptation to different realistic parameter changes is simulated: First, friction parameters f_{C} and f_{V} are increased, and in a second scenario supply pressure p_{h} is falling off. For the latter, the resulting holding force, transition and switching time over 16 adaptation cycles are shown in Figure 8. After reducing the supply pressure from $7\,\mathrm{bar}$ to $5\,\mathrm{bar}$ prior to the second cycle, the holding force collapses before the adaptation mechanism reacts with a larger shifting time thus restoring the required force of $50\,\mathrm{N}$.

Both, experimental and simulation findings, look promising in terms of the control law adapting to a significant parameter change, suggesting that the proposed policy is applicable when trying to improve energy efficiency, transition velocity, and robustness of a compressed air unit at the same time. Furthermore, it should be noted that the suggested method only requires

knowledge of the chamber pressures to estimate the stationary holding force and the corresponding constraint. Apart from that, no additional sensors are needed. Additionally, this adaptation pattern enables automatic optimization of switching points for a large number of cylinders, avoiding individual tuning. This shows practicability of the proposed approach and its ability to save manufacturers valuable engineering time.

4 Minimizing the Energy Consumption of Pressurized-air Networks

Usually, industrial plants use the industrial supply pressure to pressurize actuators. However, not every pneumatic cylinder requires such a high supply pressure to operate. As an energy-saving measure, pressure-reducing valves between supply pressure and actuator are applied to reduce compressed air intake. In this chapter, two structural improvements on how to reduce energy consumption are introduced. The first structural change assigns actuators to valve terminals in a specific cluster in Section 4.1 which is then followed by a cascaded structure that reuses exhausted air in Section 4.2. Furthermore, in Section 4.3, the adaptation law presented in Section 3.2.2 is applied to a whole pressurized-air network. Finally, combinations of these methods are examined in Section 4.4. The measurements in this section are carried out in cooperation with *Xenon Automatisierungstechnik GmbH*, a manufacturer of industrial plants. They provide and operate an industrial plant demonstrator that is commercially used in a slightly different variation by one of their clients. The demonstrator is equipped with additional sensors for validation purposes. In this way, the presented methods are tested on a real production plant without disturbing a real production line. Note that more detailed results and discussions can be found in [54, 59].

4.1 Structural Energy Saving Measures at Plant Level

To save energy in pressurized-air networks, pressure zones within the production plant are introduced and optimized. In this scenario it is assumed that n_{T} valve terminals are used to provide pressurized air and thus the n_{A} pneumatic actuators have to be assigned to a specific terminal. Given this setting, the most intuitive way to save energy is to sort the actuators by their minimum required pressure level and use this order to attach the actuators to the available terminals. The pressure level of each single terminal is then chosen based on the actuator with the highest pressure level. However, from

an energy point of view, it might be more efficient to assign an actuator to a higher pressure level, if the pressure level of the plant is thereby reduced or another actuator that is used more frequently can be added to a lower pressure level. This potentially leads to an overall reduction of pneumatic air consumption. The assignment of actuator i_A to valve terminal j_T is described by an adjacency matrix [54, 59]

$$\boldsymbol{N} = \begin{bmatrix} N_{11} & \dots & N_{1n_\mathrm{T}} \\ \vdots & \ddots & \vdots \\ N_{n_\mathrm{A}1} & \dots & N_{n_\mathrm{A}n_\mathrm{T}} \end{bmatrix}, \tag{22}$$

where $N_{i_\mathrm{A}j_\mathrm{T}} = 1$ if actuator i_A is attached to valve terminal j_T and $N_{i_\mathrm{A}j_\mathrm{T}} = 0$ else. With this matrix, the supply pressure of actuator i_A is computed as

$$p_{\mathrm{h},i_\mathrm{A}} = \sum_{j_\mathrm{T}=1}^{n_\mathrm{T}} N_{i_\mathrm{A}j_\mathrm{T}} p_{j_\mathrm{T}}. \tag{23}$$

For solving the assignment problem in an adequate way, the following simplifying assumptions are made:

- The diameter and minimum required pressure $\bar{p}_{i_\mathrm{A}}$ of each cylinder i_A are known.
- The pressure $\bar{p}_{i_\mathrm{A}}$ satisfies the requirements of the cylinder.
- The impact energy of the piston inside the cylinder is neglected.
- The pressure supply is constant and pressure changes are isothermal.

Based on these prerequisites, the assignment problem is formulated as the following optimization problem [59]

$$\min_{N_{i_\mathrm{A}j_\mathrm{T}} \in \{0,1\}} \quad \sum_{i_\mathrm{A}=1}^{n_\mathrm{A}} J_{i_\mathrm{A}}\left(p_{\mathrm{h},i_\mathrm{A}}\right) \tag{24a}$$

$$\text{s.t.} \quad \sum_{j_\mathrm{T}=1}^{n_\mathrm{T}} N_{i_\mathrm{A}j_\mathrm{T}} = 1, \qquad i_\mathrm{A} = 1, \dots, n_\mathrm{A} \tag{24b}$$

$$\sum_{i_\mathrm{A}=1}^{n_\mathrm{A}} N_{i_\mathrm{A}j_\mathrm{T}} \leq n_{\max,j_\mathrm{T}}, \qquad j_\mathrm{T} = 1, \dots, n_\mathrm{T}. \tag{24c}$$

The cost function in Equation (24a) is described as the sum of all pressurized-air consumptions $J_{i_\mathrm{A}}(p_{\mathrm{h},i_\mathrm{A}})$ of all actuators, defined in (14). Based on the

assumptions above, p_{j_T} in Equation (23) is computed by taking the maximum of all minimum required pressure values $\bar{p}_k$ for all actuators k attached to valve terminal j_T

$$p_{j_\mathrm{T}} = \max_k (\bar{p}_k | N_{kj_\mathrm{T}} = 1). \tag{25}$$

Each actuator can only be connected to one terminal, which is ensured by (24b) and each terminal j_T can only supply a finite number of actuators $n_{\max,j_\mathrm{T}}$ (24c). The optimization problem (24) is similar to a generalized assignment problem and is therefore solved by the Tabu search algorithm [54], which is a heuristic iterative search algorithm. In some cases, it may not be possible to connect actuators to arbitrary terminals if they are too far away. In this situation, additional punishments for these actuators can be added to the cost function (24a), which weigh the distance between actuators and valve terminals [54, 59].

The optimization method is validated on the industrial plant demonstrator described in [59]. The measurement results show a clear reduction of the compressed-air consumption, as depicted in Figure 9.

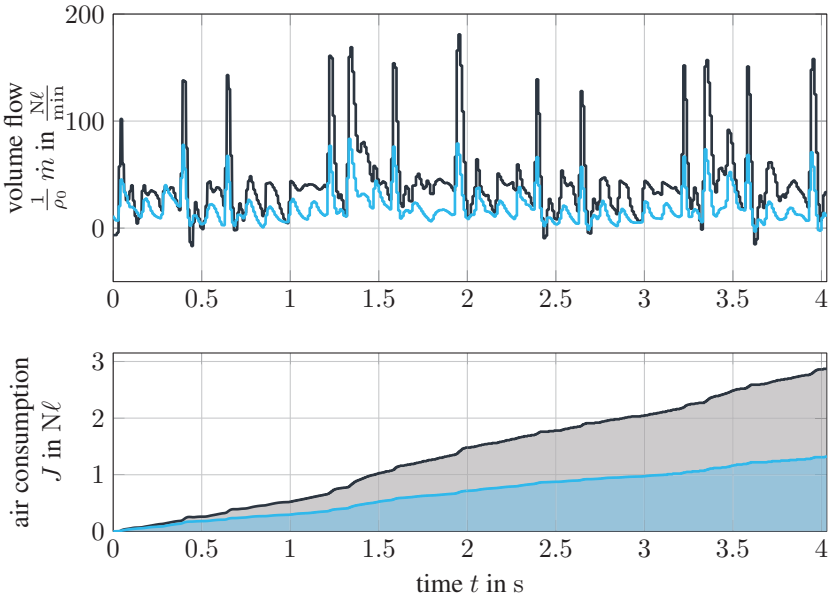

Figure 9 Measurements for optimized pressure zones. Shown are the supplied pressure flow at the top and pressurized-air-consumption at the bottom, each for the start configuration (—), as well as for the optimized configuration (—).

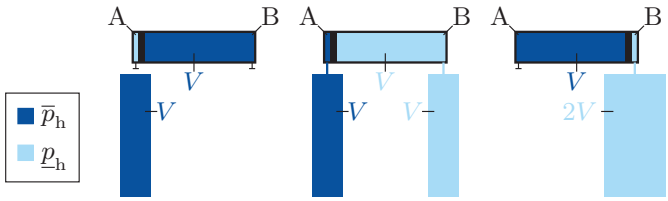

Figure 10 Illustration of cascaded-air usage for isothermal processes with the pressures $\overline{p}_\mathrm{h} = 2\underline{p}_\mathrm{h}$.

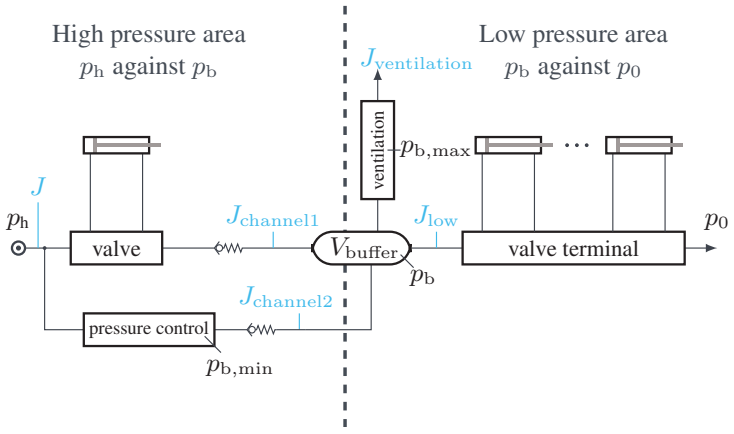

Figure 11 Components merged to ventilation cascade.

4.2 Cascaded Air Usage

In Section 4.1, multiple pressure zones have been established. To realize the different pressure levels, pressure-reducing valves are used to relax the pressure from a high level $\overline{p}_\mathrm{h}$ to a lower level $\underline{p}_\mathrm{h} > p_0$. These valves reduce air consumption, however, there remains a loss of energy potential due to the venting of the cylinder chamber. Therefore, a cascaded structure to utilize this exergy by using the pressure difference between $\overline{p}_\mathrm{h}$ and $\underline{p}_\mathrm{h}$ is proposed.

In order to give an understanding of the idea, the following thought experiment is analyzed: Assume an isothermal process and a cylinder with chamber volume V without piston rod, which is powered by $\overline{p}_\mathrm{h}$ and working against $\underline{p}_\mathrm{h}$. For the process in Figure 10 it is assumed that $\overline{p}_\mathrm{h} = 2\underline{p}_\mathrm{h}$. At first, chamber B is powered and filled by $\overline{p}_\mathrm{h}$. Next, chamber B is vented to $\underline{p}_\mathrm{h}$ into a tank of volume V while chamber A is filled by $\overline{p}_\mathrm{h}$. Due to the assumption of an isothermal process, the volume in chamber B plus tank is hereby doubled.

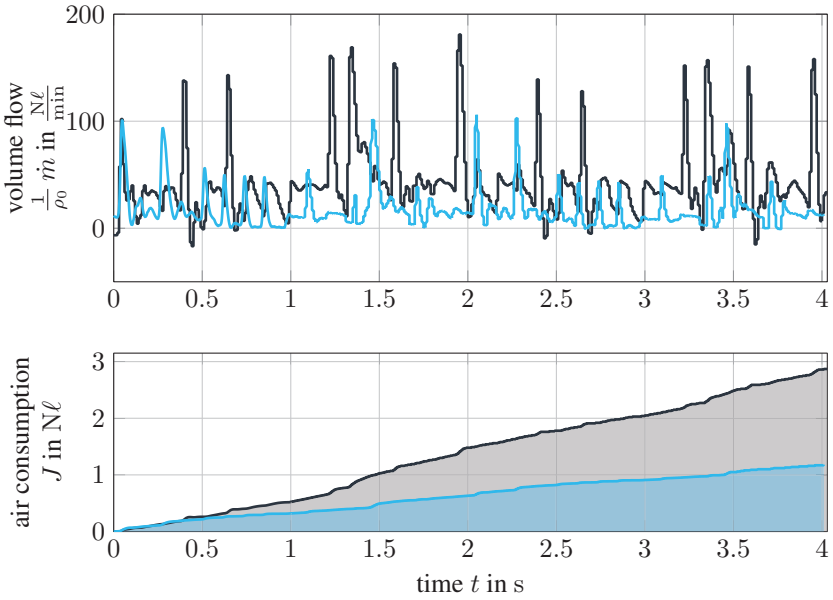

Figure 12 Measurements for cascaded structures. Shown are the supplied pressure flow at the top and pressurized air consumption at the bottom, each for the start configuration (—), as well as for the cascaded configuration (—).

Eventually, the expansion process is completed and the piston is on the right side. For the sake of this thought experiment, it is assumed that the tank volume is variable and hence the volume V of pressure $\overline{p}_\mathrm{h}$ yields volume $2V$ of pressure $\underline{p}_\mathrm{h}$. So instead of venting the cylinder to p_0, these $2V$ of pressure $\underline{p}_\mathrm{h}$ are now available to power other actuators that require a lower pressure level. The cascaded structure is divided into two pressure levels, i.e., cylinders powered by p_h and cylinders powered by a buffer pressure p_b, as illustrated in Figure 11. The buffer pressure p_b is bounded from above by $p_{\mathrm{b,max}}$ (ventilation) and from below by $p_{\mathrm{b,min}}$ (pressure control). Given this structure the cylinders have to be assigned to a pressure level such that the overall air consumption is minimized. In this Section, it is assumed that after the cycle time T all components are again in their initial state. This is a typical assumption for production lines, that operate at a certain frequency. The air consumption is consider with respect to the cycle time T. To operate as energy efficient as possible, it is demanded that there is no ventilation, i.e.,

$$J_\mathrm{ventilation} = 0. \tag{26}$$

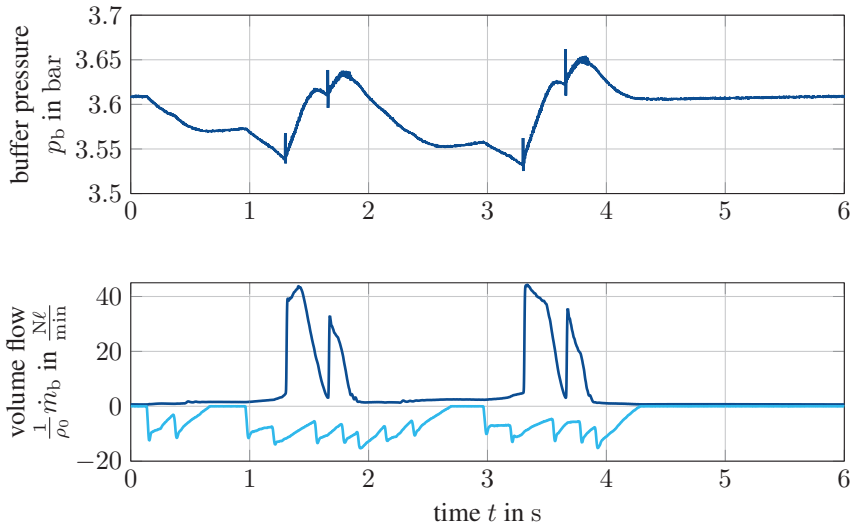

Figure 13 Measurements for the buffer pressure at the top and pressure flow towards (—) and out of (—) the buffer volume at the bottom. The optimized buffer pressure is 3.7bar.

If the buffer pressure p_b remains the same during each cycle of the cylinder, it holds that

$$J = J_\mathrm{channel1} + J_\mathrm{channel2} = J_\mathrm{low} + J_\mathrm{ventilation} \overset{(26)}{=} J_\mathrm{low}. \tag{27}$$

Due to the check valves in channel 1 and 2,

$$J_\mathrm{channel1} \geq 0, \tag{28}$$
$$J_\mathrm{channel2} \geq 0, \tag{29}$$

holds. Plugging (29) into (27) yields

$$J_\mathrm{low} \geq J_\mathrm{channel1}, \tag{30}$$

which means that the exhaust air flow of the high pressure cylinders should be smaller than, or ideally equal to, the consumption of the low pressure cylinders. Otherwise, the pressure in the buffer volume would rise which would cause the need to vent the buffer volume and thus violate (26). Note that if (26) holds, only the actuators in the low-pressure area contribute to the overall air consumption and the actuators in the high pressure area operate for 'free'.

If the high pressure area is modeled as a valve terminal denoted by index $j_\mathrm{T} = 1$ the assignment problem is defined as a more sophisticated version of problem (24):

$$\min_{N_{i_\mathrm{A} j_\mathrm{T}}, p_\mathrm{b}} \quad \sum_{i_\mathrm{A}=1}^{n_\mathrm{A}} (1 - N_{i_\mathrm{A}1})\, J_{i_\mathrm{A}}(p_\mathrm{b}) \tag{31a}$$

$$\text{s.t.} \quad p_\mathrm{b} \leq p_\mathrm{b,max} \tag{31b}$$

$$J_\mathrm{low} \geq J_\mathrm{channel1} \tag{31c}$$

$$\max_{i_\mathrm{A}}(p_{\mathrm{b},i_\mathrm{A}} | N_{i_\mathrm{A} j_\mathrm{T}} = 1) \leq p_\mathrm{b}, \qquad j_\mathrm{T} = 2, \ldots, n_\mathrm{T} \tag{31d}$$

$$\sum_{j_\mathrm{T}=1}^{n_\mathrm{T}} N_{i_\mathrm{A} j_\mathrm{T}} = 1, \qquad i_\mathrm{A} = 1, \ldots, n_\mathrm{A} \tag{31e}$$

$$\sum_{i_\mathrm{A}=1}^{n_\mathrm{A}} N_{i_\mathrm{A} j_\mathrm{T}} \leq n_{\mathrm{j_T,max}}, \qquad j_\mathrm{T} = 1, \ldots, n_\mathrm{T}. \tag{31f}$$

Since the exhaust air of the high pressure area is reused, only actuators in the low-pressure area are taken into account in (31a). The upper bound of the buffer pressure $p_\mathrm{b,max}$ in (31b) is determined by computing the pressure difference which is necessary to power the actuators in the high pressure area. Given that actuator i_A requires at least the pressure $p_{\mathrm{b},i_\mathrm{A}}$ to operate, condition (31d) guarantees that p_b satisfies the movement requirements of all cylinders in the low pressure area. Note that this condition should be conservative to make up for any model plant mismatch. Conditions (31e) and (31f) define the actuator-terminal assignment and are already known from the problem definition in (24).

The volume of the buffer V_buffer has an impact on the cylinder dynamics, since smaller buffer volumes cause a higher fluctuating buffer pressure p_b. To determine the buffer volume, the following efficient dimensioning method is proposed:

1. Assume a large buffer volume $V_\mathrm{buffer} \to \infty$ and determine assignments as well as the pressure p_b by solving (31).
2. Determine V_buffer, such that it is large enough and does not influence the pressure dynamics.

Applying the cascaded structure to the same demonstrator as in Section 4.1 results in an even better reduction of pressurized air consumption, than pressure zones do, as can be seen in the measurements shown in Figure 12.

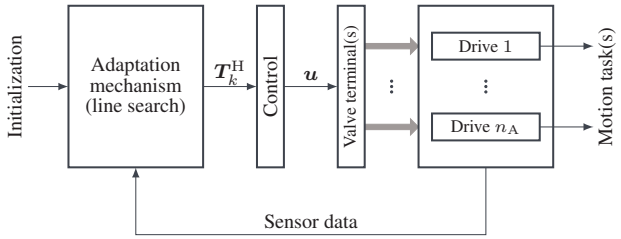

Figure 14 Schematic online adaptation of actuators at plant level, see [59]. Note that $\boldsymbol{u}$ describes the valve position for all actuators.

Note that the demonstrator is an industrial plant where the parameters are not as exactly known as the parameters of an laboratory set up. Therefore, the optimized target buffer pressure $p_{\mathrm{b}} = 3.7\,\mathrm{bar}$ and the measured buffer pressure slightly differ by $\approx 0.1\mathrm{bar}$ which is caused by these uncertainties. As desired, the buffer pressure p_{b} is nearly constant and the pressure flows towards and out of the buffer volume cancel each other out, which is shown in Figure 13. This means that $J_{\mathrm{channel2}} \approx 0$, as well as $J = J_{\mathrm{low}} \approx J_{\mathrm{channel1}}$.

4.3 Online Adaptation

This section describes how the online adaptation law from Section 3.2.2 for one cylinder is modified such that it is applicable to a whole pneumatic network. The overall schematics of the online adaptation process is shown in Figure 14: At first, switching points are initialized and then adapted to T_k^{H} using a line-search algorithm based on measured data. Then, control strategy A is used in order to generate the signal, which is applied onto the valve terminals. For the demonstrator, it is assumed that all cylinders are decoupled. To detect whether a cylinder satisfies its requirements, the pressure is measured and then used to compute the actuator force. This force must be higher than the static friction in order for the cylinder to expand. Finally, a limit switch is used to measure transition times.

This online control adaptation is applicable without much effort, since only a stationary end position force is needed for implementation. Furthermore, no parameter identification has to be applied, since the line-search algorithm is model-free.

Implementing the online adaptation on the industrial plant demonstrator yields the results shown in Figure 15, which indicate a strong reduction of pressurized air consumption. The respective pressurized air consumptions w. r. t. adaptation cycles are shown in Figure 16. As can be seen, the online

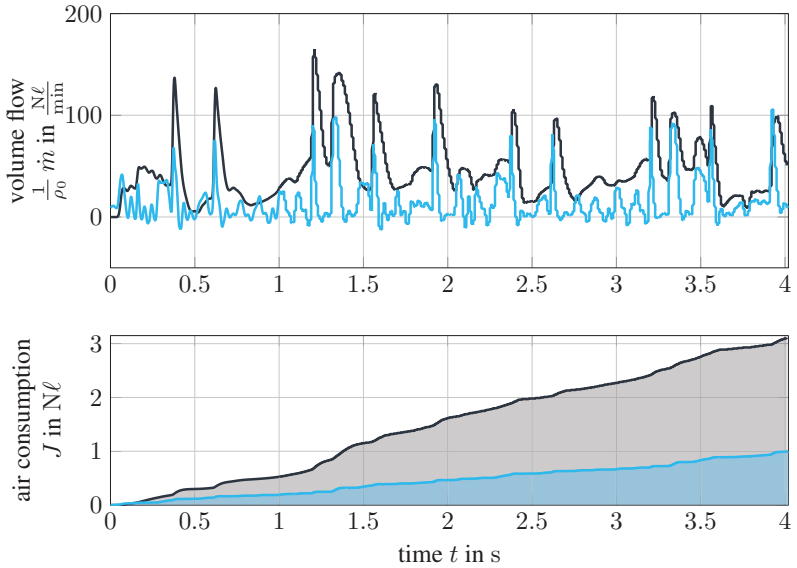

Figure 15 Measurements of initial pressure consumption (—) and pressure consumption after 56 adaptation cycles (—) [59].

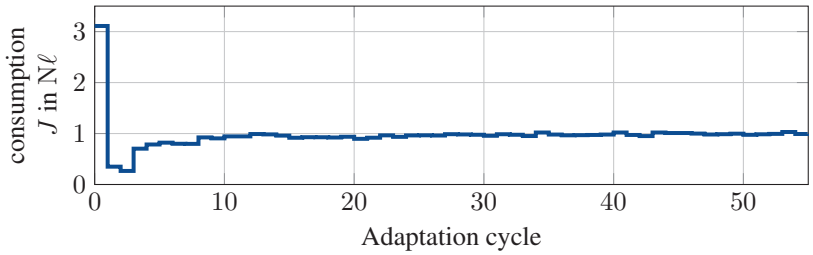

Figure 16 Consumption of pressurized air in dependency of the number of adaptation cycles [54, 59].

control strategy is aggressive, since all switching times decrease quickly when using a line-search algorithm.

4.4 Comparison and Combination of Structural Measures and Online Adaptation

The online control pattern adaptation from Section 4.3 can be either combined with the multiple pressure zones described in Section 4.3 or the cascaded air usage from Section 4.2.

Table 3 Comparison of the experimental energy consumption and savings of the proposed methods. Combination refers to the cascaded air usage and the adaptive control law applied together

	Consumption in $\mathrm{N}\ell$	Savings in %
Standard	2.87	–
Optimized pressure zones	1.32	54
Cascaded air usage	1.17	59
Adaptive control law	1.00	65
Combination	0.92	68

However, combining pressure zones with online adaptation does not result in more energy savings. In fact, adding pressure zones to online adaptation results in the same energy consumption as online adaptation on its own. This is explained by the fact that reducing the supplied pressure at valve terminals leaves less exergy potential for online adaptation.

Combining the cascaded structure with online adaptation yields better results than using either method alone. This is the case since the online adaptation is able to exploit the exergy more efficiently for cascaded structures [59].

Table 3 presents the results of the compressed air consumption of the industrial standard method, all three single measures, and the combination of online adaptation and the cascaded air usage.

In the following the obtained results are discussed and the findings of [54] are extended. In order to determine whether the proposed approach is worth implementing, the additional hardware cost and implementation effort is usually compared against the potential energy savings. However, companies are sensitive to changes in their production lines, as a production stop immediately causes additional costs. Thus, user acceptance plays an important role which is in line with experience of the authors.

The optimized pressure zones approach is the most simple strategy and only requires pressure-reducing valves. Especially if the geometric distance is included in the optimization problem, complex interconnections can be avoided. Further, it has the highest user acceptance since the fall back method is to simply increase the pressure to the previous level. Although, it has the smallest saving potential of all methods, the absolute saving potential of more than 50% is significant. Therefore, this should be the default method if no expert user is available.

The structure of the cascaded configuration is more complex and requires additional valves, throttles, pressure regulators as well as a buffer volume.

From an energetic point of view, this method is preferable in comparison to the optimized pressure zones. The cascaded configuration also does not affect the dynamic behavior of the actuators due to the way the structure is set up by guaranteeing a minimal pressure in the buffer volume. Further, the additional components are known to the pneumatic operator, which further increases the user acceptance. However, the implementation requires an expert user able to understand the cascaded concept, which might be a stepping stone in comparison to the optimized pressure zones.

The largest saving potential of all single methods was achieved using the adaptive control law since each motion task is adjusted individually. As the automatism comes as a black-box algorithm the implementation effort is comparably low. However, this might also be a problem for user acceptance since the control strategy is unknown or not understood and thus the user might not be able to perform debugging, which is crucial in production lines. This means that the fear of not being able to handle potential problems from the algorithm might be a criterion for exclusion. The algorithm further requires the appropriate valve technology, processors and sensors which further hinders user acceptance. Although, this method is a plug and play approach in theory, it might only be used if an expert is available who can fix potential problems due to the low user acceptance.

Finally, the combination of the adaptation law and the cascaded configuration yields an additional 3% saving potential compared to solely using the adaptation law. Although the best results were achieved this way, the drawbacks are also joined. These are the combined hardware costs as well as the requirement of an expert user and the drawback of not being able to debug the black-box algorithm. Thus, the combination is only recommended if energy saving is the sole criterion. Otherwise, either the adaptation law or the cascaded configuration is recommended.

5 Summary and Conclusions

This work was concerned with the energy saving potential of compressed air systems. First, in-depth models of the components of individual drives were introduced: A mechanical and thermodynamical model of pneumatic cylinders was used to describe the dynamics of the piston position and chamber pressure, before modeling of valves and tubes was considered. Optimal dimensioning parameters for a single pneumatic cylinder were found using a proposed gradient-based optimization algorithm and the derived model. Additionally, different control strategies were tested and as an extension to

this concept, an adaptive control law, automatically adjusting the switching times, was presented. This resulted in increased energy efficiency through an enhanced motion profile, while at the same time offering improved robustness against uncertainties in the task parameters. Since production plants typically operate multiple drives simultaneously, energy saving methods on the level of pressurized air networks were investigated next. Apart from the aforementioned adaptation mechanism, which is also applicable to entire production plants, optimized pressure zones and cascaded air usage as well as combinations of the three were discussed. The latter two make use of an improved distribution of the supply pressure by sorting the actuators in terms of required pressure level or reusing exhausted air, respectively.

All proposed measures were tested and compared against state-of-the-art strategies using simulation and experimental results and showed significantly improved performance. Further, the experiments were performed on an industrial plant demonstrator. The developed methods provide the possibility to reduce consumption of compressed air applications in the industry by more than 60% and are applicable in an easy and automated fashion. An overview of the energy savings for each method is presented in Table 3.

Acknowledgement

The recent results, which are presented in this article, are part of EnAP-project (`http://www.enap-projekt.de`) and were supported by the German Federal Ministry for Economic Affairs and Energy (Grant 03ET1385B: User oriented use of energy-efficient drive technology in production. Original title, in German: *Anwenderorientierter Einsatz energieeffizienter Antriebstechnik in der Produktion*).

Symbols and Variables

Symbol	Description
$\boldsymbol{N}$	adjacency matrix
J	air consumption
ρ_0	air density
α	angle of mounting orientation

(*Continued*)

Continued

Symbol	Description
$\dot{U}_i$	change of the internal energy of chamber i
b	critical pressure ratio
β	constant for the contact force model
γ	constant for the contact force model
δ	constant for the contact force model
f_{C}	Coulomb friction coefficient
$A,\ A_i$	cross section, piston area of chamber i
l	cylinder length
d	cylinder diameter
$v^*_{j_{\mathrm{P}}}$	demanded (maximal) impact velocity for process j_{P}
$T^*_{j_{\mathrm{P}}}$	demanded (maximal) transition time for process j_{P}
$F^*_{\mathrm{H},j_{\mathrm{P}}}$	demanded (minimal) holding force for process j_{P}
ρ	density of the fluid
$\boldsymbol{\zeta}$	design parameters
$\dot{H}_i$	change of the enthalpy of chamber i
ψ	flow function
F_i	force; holding H, terminal T, friction F, gravitational G
g	gravity
c_p	heat capacity for constant pressure
c_v	heat capacity for constant volume
$\dot{Q}_i$	heat flow of chamber i
α_T	heat transfer coefficient
$\tilde{\boldsymbol{h}}$	inequality constraints
κ	isentropic exponent
M	load mass
$\dot{m},\ \dot{m}_i$	mass flow; in chamber i, of buffer b
n_{A}	number of actuators
$\ddot{s}$	piston acceleration
s	piston position
$\dot{s}$	piston velocity
n	polytropic exponent
$\dot{m}_i^+$	positive shares of the mass flow in chamber i
p_i	pressure; of chamber i; ambient 0, supply h, buffer b
$\boldsymbol{S}$	sensitivity
δ_{S}	shape parameter for the friction force model
C	sonic conductance
R_L	specific gas constant
c	speed of sound

(*Continued*)

Continued

Symbol	Description
$\boldsymbol{x}$	state of the system
f_{S}	Stribeck friction coefficient
ν_{G}	Stribeck velocity
$T_i^{\mathrm{H}}, T_i^{\mathrm{L}}$	switching times of chamber i
$\boldsymbol{\Phi}$	task parameters
θ_i	temperature; of chamber i; ambient 0
ν_{G}	transition velocity
u_i, $\boldsymbol{u}$	valve position of chamber i; vector of
v	velocity of the fluid
f_{V}	viscous friction coefficient
V_i	volume of chamber i
$\dot{W}_i$	work for volume change of chamber i

References

[1] German Environment Agency. Energy consumption by sector. https://www.umweltbundesamt.de/daten/energie/energieverbrauch-nach-energietraegern-sektoren#entwicklung-des-endenergieverbrauchs-nach-sektoren-und-energietragern, 2020. Accessed: 2022-01-31.

[2] T. Javied, T. Rackow, R. Stankalla, C. Sterk, and J. Franke. A study on electric energy consumption of manufacturing companies in the german industry with the focus on electric drives. *Procedia CIRP*, 41:318–322, 12 2016.

[3] Deutsche Energie-Agentur GmbH (dena). Energieeffizienz in kleinen und mittleren Unternehmen. https://www.dena.de/fileadmin/dena/Dokumente/Pdf/1419_Broschuere_Energieeffizienz-in-KMU_2015.pdf, 2015. Accessed: 2022-02-07.

[4] Y. Wang, K. Ueda, and S. A. Bortoff. A hamiltonian approach to compute an energy efficient trajectory for a servomotor system. *Automatica*, 49(12):3550–3561, 2013.

[5] S. Merkelbach, H. Murrenhoff, C. Brecher, M. Fey, and B. Eßer. Pneumatische und elektro-mechanische Linearantriebe - Ein Vergleich der TCO. *Olhydraulik und Pneumatik*, 2017:42–49, 09 2017.

[6] E. Rakova and J. Weber. Exonomy analysis for the selection of the most cost-effective pneumatic drive solution. In *9th FPNI Ph. D. Symposium*

on Fluid Power. American Society of Mechanical Engineers Digital Collection, 2016.

[7] E. Rakova, J. Hepke, and J. Weber. Exonomy analysis for the inter-domain comparison of electromechanical and pneumatic drives. In *Proceedings of the 10th International Fluid Power Conference, Dresden, Germany*, pages 8–10, 2016.

[8] R. Enparantza, O. Revilla, A. Azkarate, and J. Zendoia. A life cycle cost calculation and management system for machine tools. In *13th CIRP international conference on life cycle engineering*, volume 2, pages 717–722, 2006.

[9] M. Barkmeyer, A. Kaluza, N. Pastewski, S. Thiede, and C. Herrmann. Integration of stakeholder perspectives for development of sustainable automation components. *Procedia CIRP*, 48:388–393, 2016.

[10] Y. Shi, M. Cai, W. Xu, and Y. Wang. Methods to evaluate and measure power of pneumatic system and their applications. *Chinese Journal of Mechanical Engineering*, 32(1):1–11, 2019.

[11] M. Rückert, S. Merkelbach, R. Alt, and K. Schmitz. Online life cycle assessment for fluid power manufacturing systems–challenges and opportunities. In *IFIP International Conference on Advances in Production Management Systems*, pages 128–135. Springer, 2018.

[12] S. Merkelbach, K. Schmitz, and H. Murrenhoff. *Analysis of the economic and ecological properties of pneumatic actuator systems with pneumatic transformers*. Number RWTH-2020-01561. Lehrstuhl und Institut für fluidtechnische Antriebe und Steuerungen, 2020.

[13] R. Neumann and M. Doll. How big is the efficiency of pneumatic drives? An experiment provides clarity! In *Modern Fluid Power - Challenges, Responsibilities, Markets, IFK, International Fluid Power Conference, 9, Modern Fluid Power - Challenges, Responsibilities, Markets, IFK, Internationales Fluidtechnisches Kolloquium, 9*, pages 328–339, Aachen, 2014. HP-Fördervereinigung Fluidtechnik;.

[14] S. Hirzel, T. Hettesheimer, and M. Schröter. Electric or pneumatic - comparing electric and pneumatic linear dives with regard to energy efficiency and costs. *European Council for an Energy-Efficient Economy (ECEEE Industrial Summer Study)*, pages 475–484, 2014.

[15] S. Merkelbach, H. Murrenhoff, M. Fey, and B. Eßer. Pneumatic or electromechanical drives – a comparison regarding their exergy efficiency. 2016.

[16] W. Gauchel. Energiesparende Pneumatik – Konstruktive sowie schaltungs- und regelungstechnische Ansätze. *O+P*, pages 33–39, 2006.

[17] P. Harris, G. E. O'Donnell, and T. Whelan. Energy efficiency in pneumatic production systems: state of the art and future directions. *Leveraging technology for a sustainable world*, pages 363–368, 2012.

[18] Parker-Hannifin Corporation. Pneumatic actuator products – cylinders, guided cylinders and rotary actuators. catalog 0900p-6. https://www.parker.com/literature/Literature%20Files/pneumatic/Literature/Actuator-Cylinder/0900/0900P_Complete.pdf, 2016. Accessed: 2021-25-02.

[19] AVENTICS GmbH. Technical information – supplement to the pneumatics catalog. www.aventics.com/uploads/mediadb/data/DOC/org/R412019128_2014-09-EN_TI-Katalog.PDF, 2018. Accessed: 2021-25-02.

[20] SMC Pneumatics (UK) Ltd. The pneu book. www.smc.eu/portal_ssl/WebContent/local/UK/Pneu_Book/pneubook.pdf. Accessed: 2021-25-02.

[21] S. Berchten and C. Ritz. Replacement of pneumatic and hydraulic drives with electrical drives-analysis of potential; Ersatz von pneumatischen und hydraulischen Antrieben durch Elektroantriebe. Potentialanalyse. 2006.

[22] R. Gloor. Energy savings in Swiss compressed-air installations; Energieeinsparungen bei Druckluftanlagen in der Schweiz. 2000.

[23] F. Ilmberger and F. Seyfried. Druckluftversorgungskonzepte für Industriebetriebe. *Brennstoff Wärme Kraft*, 46:398–398, 1994.

[24] W. Bader and K. Kissock. Exergy analysis of industrial air compression. In *National Industrial Energy Technology Conference*, volume 22, pages 89–98. Texas A&M University, 2000.

[25] S. Krichel, S. Hülsmann, S. Hirzel, R. Elsland, and O. Sawodny. Mehr Klarheit bei der Druckluft. Exergieflussdiagramme als neue Grundlage für Effizienzbetrachtungen bei Druckluftanlagen. *Zeitschrift für Ölhydraulik und Pneumatik*, 56:1–2, 2012.

[26] E. Rakova and J. Weber. Process simulation of energy behaviour of pneumatic drives. *Procedia Engineering*, 106:149–157, 2015.

[27] P. Harris, S. Nolan, and G. E. O'Donnell. Energy optimisation of pneumatic actuator systems in manufacturing. *Journal of Cleaner Production*, 72:35–45, 2014.

[28] J. Hepke and J. Weber. Energy saving measures on pneumatic drive systems. In *13th Scandinavian International Conference on Fluid Power; June 3-5; 2013; Linköping; Sweden*, number 092, pages 475–483. Linköping University Electronic Press, 2013.

[29] M. Doll, R. Neumann, and O. Sawodny. Dimensioning of pneumatic cylinders for motion tasks. *International Journal of Fluid Power*, 16, 2015.

[30] M. Doll. *Optimierungsbasierte Strategien zur Steigerung der Energieeffizienz pneumatischer Antriebe*. Shaker Verlag, 2016.

[31] V. Vigolo and V. J. De Negri. Sizing optimization of pneumatic actuation systems through operating point analysis. *Journal of Dynamic Systems, Measurement, and Control*, 143(5), 2021.

[32] VDI/VDE 3548. Antriebe in der Handhabung- und Montagetechnik. Auswahlkriterien und Energieeffizienz in linearen Einzelbewegungen. 2018.

[33] J. Wang and T. Gordon. Energy-efficient tracking control of pneumatic cylinders. In *2011 50th IEEE Conference on Decision and Control and European Control Conference*, pages 7956–7961. IEEE, 2011.

[34] X. Shen and M. Goldfarb. Energy Saving in Pneumatic Servo Control Utilizing Interchamber Cross-Flow. *Journal of Dynamic Systems, Measurement, and Control*, 129(3):303–310, 10 2006.

[35] A. Hildebrandt, R. Neumann, and O. Sawodny. Optimal system design of SISO-servopneumatic positioning drives. *IEEE transactions on control systems technology*, 18(1):35–44, 2009.

[36] A. Hildebrandt and O. Sawodny. Trajectory generation and sizing of servopneumatic SISO-drives). *at-Automatisierungstechnik*, 55(2):75–85, 2007.

[37] V. Blagojević, D. Šešlija, M. Stojiljković, and S. Dudić. Efficient control of servo pneumatic actuator system utilizing by-pass valve and digital sliding mode. *Sadhana*, 38(2):187–197, 2013.

[38] E. J. Barth, J. Zhang, and M. Goldfarb. Sliding mode approach to pwm-controlled pneumatic systems. In *Proceedings of the 2002 American Control Conference (IEEE Cat. No. CH37301)*, volume 3, pages 2362–2367. IEEE, 2002.

[39] L. Endler, V. J. De Negri, and E. B. Castelan. Compressed air saving in symmetrical and asymmetrical pneumatic positioning systems. *Proceedings of the Institution of Mechanical Engineers, Part I: Journal of Systems and Control Engineering*, 229(10):957–969, 2015.

[40] K. Ahn and S. Yokota. Intelligent switching control of pneumatic actuator using on/off solenoid valves. *Mechatronics*, 15(6):683–702, 2005.

[41] A. Pfeffer, T. Glück, and A. Kugi. Soft landing and disturbance rejection for pneumatic drives with partial position information. *IFAC-PapersOnLine*, 2016.

[42] H. Du, C. Hu, W. Xiong, Z. Jiang, and L. Wang. Energy optimization of pneumatic actuating systems using expansion energy and exhaust recycling. *Journal of Cleaner Production*, 254:119983, 2020.

[43] K. Janiszowski and M. Kuczyński. Energy saving control in low cost pneumatic positioning systems. In *2010 15th International Conference on Methods and Models in Automation and Robotics*, pages 61–66. IEEE, 2010.

[44] M. Y. Yusop. *Energy saving for pneumatic actuation using dynamic model prediction*. Cardiff University, 2006.

[45] S. Merkelbach and H. Murrenhoff. Exergy based analysis of pneumatic air saving measures. In *ASME/BATH 2015 Symposium on Fluid Power and Motion Control*. American Society of Mechanical Engineers Digital Collection, 2015.

[46] M. Doll, R. Neumann, and O. Sawodny. Energy efficient use of compressed air in pneumatic drive systems for motion tasks. In *Proceedings of 2011 International Conference on Fluid Power and Mechatronics*, pages 340–345. IEEE, 2011.

[47] M. Doll, O. Sawodny, and R. Neumann. Energy efficient adaptive control of pneumatic drives with switching valves. In *Proc. from the 7th International Fluid Power Conference, Dresden*, 2012.

[48] R. Parkkinen and P. Lappalainen. A consumption model of pneumatic systems. In *Conference Record of the 1991 IEEE Industry Applications Society Annual Meeting*, pages 1673–1677. IEEE, 1991.

[49] K. Hyvarinen and P. Lappalainen. A novel simulator of pneumatic networks. In *Proceedings of the IEEE International Conference on Industrial Technology (ICIT'96)*, pages 343–347. IEEE, 1996.

[50] P. Harris, G. E. O'Donnell, and T. Whelan. Predictive consumption models for electropneumatic production systems. *IEEE/ASME Transactions on Mechatronics*, 18(5):1519–1526, 2012.

[51] J. Parkkinen and K. Zenger. A new efficiency index for analysing and minimizing energy consumption in pneumatic systems. *International Journal of Fluid Power*, 9(1):45–52, 2008.

[52] S. Krichel and O. Sawodny. Analysis and optimization of compressed air networks with model-based approaches. *Ventil*, 4(17):334–341, 2011.

[53] S. Krichel. *Komponentenmodellierung und Strukturoptimierung in industriellen Druckluftnetzen*. Shaker, 2012.

[54] A. Raisch and O. Sawodny. Energy savings in pneumatically driven plants. *IEEE/ASME Transactions on Mechatronics*, 2021.

[55] X. Luo, J. Wang, H. Sun, J. W. Derby, and S. J. Mangan. Study of a new strategy for pneumatic actuator system energy efficiency improvement via the scroll expander technology. *IEEE/ASME Transactions on Mechatronics*, 18(5):1508–1518, 2012.

[56] J. S. Leszczynski and D. Grybos. Compensation for the complexity and over-scaling in industrial pneumatic systems by the accumulation and reuse of exhaust air. *Applied Energy*, 239:1130–1141, 2019.

[57] C. von Grabe and H. Murrenhoff. Efficiency improvements by air recuperation using the example of a pick-and-place-application. In *Proceedings of the 9th JFPS International Symposium on Fluid Power,(JFPS), Matsue, Japan*, pages 361–367, 2014.

[58] J. Hepke. *Energetische Untersuchung und Verbesserung der Antriebstechnik pneumatischer Handhabungssysteme*. Shaker Verlag, 2017.

[59] A. Raisch. *Optimierungsbasierte Auslegung und Steuerung in der Pneumatik und Vergleich mit elektromechanischen Antrieben*. Shaker Verlag, 2020.

[60] H. Olsson, K. J. Åström, C. C. De Wit, M. Gäfvert, and P. Lischinsky. Friction models and friction compensation. *Eur. J. Control*, 4(3):176–195, 1998.

[61] D. Schindele and H. Aschemann. Adaptive friction compensation based on the LuGre model for a pneumatic rodless cylinder. In *Annual Conference of IEEE Industrial Electronics*, 2009.

[62] K. H. Hunt and F. R. E. Crossley. Coefficient of Restitution Interpreted as Damping in Vibroimpact. *Journal of Applied Mechanics*, 42(2):440–445, 06 1975.

[63] M. Göttert. *Bahnregelung servopneumatischer Antriebe, Berichte aus der Steuerungs- und Regelungstechnik*. PhD thesis, Zugl.: Siegen, Univ., Diss., Aachen, 2004.

[64] V. Falkenhahn. *Modellierung und modellbasierte Regelung von Kontinuum-Manipulatoren*. Shaker Verlag, 2017.

[65] T. Glück, W. Kemmetmüller, and A. Kugi. Trajectory optimization for soft landing of fast-switching electromagnetic valves. *IFAC Proceedings Volumes*, 2011.

[66] H.-P. Bala. Durchflussmessungen und strömungstechnische kenngrößen. *O+ P ölhydraulik und pneumatik*, 29:541–544, 1985.

[67] D. Rager and R. Neumann. Simplified fluid transmission line model for pneumatic control applications. *14th Scandinavian International Conference on Fluid Power*, pages 1–13, 2015.

[68] R. Kern. *Design and Experimental Validation of Output Feedback Tracking Controllers for a Pneumatic System with Distributed Parameters*. PhD thesis, Technical University of Munich, 2019.

[69] Industriebedarf Ohmert GmbH. Cylinder ISO 6432 price. https://www.pneumatikshop-online.de/de/rundzylinder-doppeltwirkend- iso-6432-zylinder-kolben-hub-pneumatikzylinder-isozylinder-iso-zyl inder.html, 2021. Accessed: 2021-03-10.

[70] A. Raisch and O. Sawodny. Analysis and optimal sizing of pneumatic drive systems for handling tasks. *Mechatronics*, 59:168–177, 2019.

[71] A. Raisch, S. Hülsmann, and O. Sawodny. Saving energy by predictive supply air shutoff for pneumatic drives. In *2018 European Control Conference (ECC)*, pages 965–970. IEEE, 2018.

[72] A. Raisch and O. Sawodny. On evaluation of planar drive kinematics for handling tasks. In *2018 IEEE Conference on Decision and Control (CDC)*, pages 5134–5139. IEEE, 2018.

[73] A. Raisch and O. Sawodny. Modeling and analysis of pneumatic cushioning systems under energy-saving measures. *IEEE Transactions on Automation Science and Engineering*, 17(3):1388–1398, 2019.

[74] A. Raisch and O. Sawodny. Adapting energy optimal trajectories for friction-afflicted electromechanical drives. *IFAC-PapersOnLine*, 50(1):770–775, 2017.

[75] A. Raisch and O. Sawodny. Consumption minimization for electromechanical drives by energy-optimal feedforward control. In *2019 IEEE International Conference on Systems, Man and Cybernetics (SMC)*, pages 1557–1562. IEEE, 2019.

[76] H. K. Khalil. *Nonlinear systems*, volume 2. 1996.

Biographies

Daniel Müller received his M.Sc. degree in Engineering Cybernetics from the University of Stuttgart, Germany, in 2018. Since spring 2018, he has been a Research Assistant with the Institute for System Dynamics, University of Stuttgart, Germany. His research interests include continuum manipulators, machine learning and optimization.

Jonathan Haag received his B.Sc. degree in Engineering Cybernetics at the University of Stuttgart, Germany, in 2021. Since 2020 he has been a student assistant with the Institute for System Dynamics, University of Stuttgart, Germany. His research interests include systems and control theory.

Jennifer Wickert received her B.Sc. degree in Simulation Technology from the University of Stuttgart, Germany, in 2019. Since 2020, she has been a Student Assistant with the Institute for System Dynamics, the University of Stuttgart, Germany. Her research interests include system dynamics and machine learning.

Adrian Raisch received the M.Sc. degree in Engineering Cybernetics from the University of Stuttgart, Germany, in 2015. He was a Research Assistant at the Institute for System Dynamics, University of Stuttgart, from 2015 until 2020, where he successfully finished his Ph.D. degree. His current research interests include modeling and control.

Kathrin Hoffmann received the M.S. degree in Engineering Science and Mechanics from the Georgia Institute of Technology, Atlanta, USA in 2018, and the M.Sc. degree in Engineering Cybernetics from the University of Stuttgart, Stuttgart, Germany in 2019. She is currently a Research Assistant with the Institute for System Dynamics, University of Stuttgart, Germany. Her research interests include the modeling and control of pneumatic drive systems as well robotics.

Kevin Schmidt received the Ph.D. degree in engineering cybernetics from the University of Stuttgart, Institute for System Dynamics, Germany, in 2020. His dissertation focused on disturbance compensation for adaptive high-power lasers. He was with the Center for Control Systems and Dynamics, UC San Diego, USA in 2016. Since 2021 he is with Robert Bosch GmbH, Corporate Sector Research and Advance Engineering. His research interests include modeling, optimization and control of distributed systems and uncertainty quantification as well as applications in the field networked and cyber-physical systems.

Oliver Sawodny received the Dipl.-Ing. degree in Electrical Engineering from the University of Karlsruhe, Karlsruhe, Germany, in 1991, and the Ph.D. degree from the Ulm University, Ulm, Germany, in 1996. In 2002, he became a Full Professor with the Technical University of Ilmenau, Ilmenau, Germany. Since 2005, he has been the Director of the Institute for System Dynamics, University of Stuttgart, Stuttgart, Germany. His current research interests include methods of differential geometry, trajectory generation, and applications to mechatronic systems.